

Mohamed F. Abd Al-Samieh ¹

Ridge geometry effect on the behavior of elastohydrodynamic lubrication of point contact problem

A numerical solution is presented to investigate the influence of the geometry and the amplitude of the transverse ridge on the characteristics of elastohydrodynamic lubrication for point contact problem under steady state condition. Several shapes of ridges with different amplitudes are used in the stationary case, such as flat-top ridge, cosine wave ridge and sharp ridge of triangular shape. Results of film thickness and pressure distributions of the aforementioned ridge feature are presented at different locations through an elastohydrodynamically lubricated contact zone for different amplitude of the ridge. Simulations were performed using the Newton-Raphson iteration technique to solve the Reynolds equation. The numerical results reveal that, to predict optimum solution for lubricated contact problem with artificial surface roughness, the geometrical characteristics of the ridge should have profiles with smooth transitions such as those of a cosine wave shape with relatively low amplitude to reduce pressure spike and therefore cause the reduction in the film thickness. The position of the location of the ridge across the contact zone and the amplitude of the ridge play an important role in the formation of lubricant film thickness and therefore determine the pressure distribution through the contact zone.

Nomenclature

A	Amplitude
b	Radius of Hertzian contact region
E	Reduced modulus of elasticity
G^*	Materials' parameter, $G^* = E'\alpha$

✉ Mohamed F. Abd Al-Samieh, e-mail: mohamed.fahmy203@hotmail.com

¹Mechanical Design & Production Department, Military Technical College, Cairo, Egypt.



© 2020. The Author(s). This is an open-access article distributed under the terms of the Creative Commons Attribution-NonCommercial-NoDerivatives License (CC BY-NC-ND 4.0, <https://creativecommons.org/licenses/by-nc-nd/4.0/>), which permits use, distribution, and reproduction in any medium, provided that the Article is properly cited, the use is non-commercial, and no modifications or adaptations are made.

h	Lubricant film thickness
H	Dimensionless film thickness, $H = hR/b^2$
H_0	Dimensionless central oil film thickness
K	Elliptical ratio
l	Dimensionless side leakage boundary distance
m	Dimensionless inlet distance
n_x, n_y	Number of computational grid nodes
p	Hydrodynamic contact pressure
P	Dimensionless hydrodynamic contact pressure, $P = p/P_{\text{Her}}$
P_{Her}	Maximum Hertzian contact pressure
R	Reduced radius of counterformal contact
u	Speed of entraining motion, $u = (u_A + u_B)/2$
U^*	Speed (or rolling viscosity) parameter, $U^* = u\eta_0/E'R^2$
w	Normal applied contact load
W^*	Load parameter, $W^* = w/E'R^2$
X, Y	Dimensionless co-ordinates, $X = x/b, Y = y/b$
x_d	Position of the located ridge
Z	Viscosity-pressure index
α	Pressure of viscosity coefficient
δ	Total elastic deformation
ε, ξ	Constants used in Eq. (3)
η	Lubricant dynamic viscosity
η_0	Atmospheric lubricant dynamic viscosity
$\bar{\eta}$	Dimensionless lubricant viscosity, $\bar{\eta} = \eta/\eta_0$
λ	Dimensionless wavelength
ρ	Lubricant density
$\bar{\rho}$	Dimensionless lubricant density, $\bar{\rho} = \rho/\rho_0$
Ω	Under-relaxation factor
Superscripts	
i, j	Contravariant influence coefficient indices
n	Iteration index
Subscripts	
k, l	Covariant influence coefficient indices

1. Introduction

The surface roughness represents an important issue concerned with many tribological problems for several decades. Roughness features in elasto-hydrodynamically lubricated contacts substantially affect minimum film thickness, pres-

sure distribution and thus have a great influence on friction, wear and fatigue life. Thanks to the improvements in computer technology, research in the field of elastohydrodynamic lubrication has gradually shifted from the steady-state smooth surface problem to more complex geometries, i.e., taking into account the effect of surface features such as dents, bumps and waviness (see Gohar and Rahnejat [1]).

Two types of approaches for rough surface of elastohydrodynamic lubrication have been used. The first approach is the stochastic method, as shown by many researchers, such as Patir and Cheng [2], Epstein et al. [3], Wang et al. [4] and Masjedi and Khonsari [5]. The other approach is the deterministic method (see for example, Hu and Zhu [6], Jacod et al. [7], Yang et al. [8] and Wang et al. [9]). Surface features can be incorporated into numerical models by assuming real or artificial surface features. While real roughness is difficult to model numerically, works dealing with artificial roughness are more widespread.

Venner and Lubrecht [10] investigated the influence of a transverse ridge on the film thickness and pressure profile in a circular elastohydrodynamic lubrication contact under rolling/sliding conditions for different location of the ridge through the contact zone using multilevel Full Approximation Scheme to obtain fast convergence of the solution. Holmes et al. [11] presented an analysis for point contact elastohydrodynamic lubrication problems using coupled elastic and hydrodynamic equations with the use of a novel differential deflection formulation. Venner and Lubrecht [10] and Holmes et al. [11] modulated the transverse ridge as a cosine wave added to one of the smooth contacting bodies. They showed that, when the ridge is completely deformed, i.e., flattened in the center of the contact and only near the edge of the contact, it affects the film thickness profile. The flattening is accompanied by a maximum pressure increase over the ridge in the center of the contact. Felix-Quinonez et al. [12, 13] studied both experimentally and numerically lubricant film thickness fluctuations introduced by a single flat-top transverse ridge passing through an elastohydrodynamically lubricated contact under pure rolling conditions. They found that the ridge geometry affects the formation of film thickness perturbations in the high-pressure region of the contact. Kaneta et al. [14], Krupka et al. [15] and Feng Wang et al. [16] used optical interferometry technique to study the transient effects of transversely-oriented moving ridges having different heights on point contact elastohydrodynamic lubricated films. They found that the ridge affects local film profiles depending on the velocity of the rough surface relative to that of the smooth surface. Ficza et al. [17] presented a numerical solution using multigrid method to solve the Reynolds equation for an isothermal elastohydrodynamic point contact with a single transverse flat-top ridge on one of the surfaces for Newtonian and non-Newtonian fluid based on Ree-Eyring model. Their results show the film thickness and pressure distributions for passage of the ridge through the contact zone. Their results conform well to experimental observations of Sperka [18]. Ali et al. [19] presented experimental and numerical investigations to study the effects of transverse limited micro-grooves on the behavior of film thickness and friction in elastohydrodynamic point contacts.

They showed that transverse shallow micro-grooves enhance significantly the film thickness of elastohydrodynamic lubrication contacts under thin film and starved conditions.

Recently, Sperka et al. [20] and Kostal et al. [21] presented extended and simple version of amplitude attenuation model for prediction of roughness effects on film thickness variations for several indentation shapes including rectangular, rounded bottom and triangular. From these simulations, they found that an optimal indentation profile should have smooth shape with appropriate width and depth. The deformed shape of the rectangular indentation has the sharpest spikes. Their numerical results agree well with their experimental work. Hultqvist et al. [22] investigated numerically the behavior of the transient event of surface feature passing through a thermal elastohydrodynamic line contact operating under different sliding conditions. They found that sliding influences the temperature rise in the contact significantly, especially in the vicinity of the asperity, and the local temperature rise mainly influences the film thickness during exiting of inlet perturbations and the asperity.

Therefore, nowadays, there is a great tendency of applying surface textures to study their effect through the lubricated contact problem. In this paper, the author investigated behavior of elastohydrodynamic lubrication of point contact problem for different geometry and amplitude of single ridge located at different position through lubricated contact zone in order to get an optimum shape of the ridge. Comparisons between the current numerical solutions and other published numerical results were made. Different geometrical characteristics of the ridge, including flat-top, cosine wave and sharp ridge of triangle shape are studied in this paper for different amplitude of the ridge. To deal with this problem, a numerical solution using Newton-Raphson technique with Gauss-Seidel iteration method to solve the Reynolds equation was developed for elastohydrodynamic lubrication of point contact problems.

2. Background theory

The two-dimensional Reynolds equation for a general non-Newtonian fluid can be written in a dimensionless form as:

$$\frac{\partial}{\partial X} \left(\frac{\bar{\rho} H^3}{\bar{\eta}} \frac{\partial P}{\partial X} \right) + \frac{1}{K^2} \frac{\partial}{\partial Y} \left(\frac{\bar{\rho} H^3}{\bar{\eta}} \frac{\partial P}{\partial Y} \right) = \lambda \frac{\partial}{\partial X} (\bar{\rho} H), \quad (1)$$

where the following dimensionless variables apply:

$$X = \frac{x}{b}, \quad Y = \frac{y}{b}, \quad \bar{\eta} = \frac{\eta}{\eta_0}, \quad \bar{\rho} = \frac{\rho}{\rho_0},$$

$$H = \frac{hR}{b^2}, \quad P = \frac{p}{P_{\text{Her}}}, \quad \lambda = \frac{12u\eta_0 R^2}{b^3 P_{\text{Her}}}.$$

The dimensionless film thickness equation can be given as:

$$H(X, Y) = H_0 + \frac{(X - m)^2}{2} + \frac{K^2(Y - l)^2}{2} + \frac{R\delta(X, Y)}{b^2} + S(X, Y), \quad (2)$$

where δ – the total elastic deformation of the contiguous bodies in contact is given as shown by Gohar and Rahnejat [1], Al-Samieh and Rahnejat [23] and Al-Samieh [24, 25]. The last term ($S(X, Y)$) in film thickness equation (2) is used to represent the geometry of the surface roughness.

The variation of density with pressure is defined by Dowson and Higginson [26] as:

$$\bar{\rho} = 1 + \frac{\varepsilon PP_{\text{Her}}}{1 + \zeta PP_{\text{Her}}}, \quad (3)$$

where the constants ε and ζ depend on the type of lubricant.

The relation of viscosity with pressure is given by Roelands [27] as:

$$\bar{\eta} = \exp [\ln \eta_0 + 9.67] \left[\left(1 + 5.1 \cdot 10^{-9} PP_{\text{Her}} \right)^Z - 1 \right],$$

where:

$$Z = \frac{\alpha}{5.1 \cdot 10^{-9} [\ln \eta_0 + 9.67]}. \quad (4)$$

The Reynolds' equation can be solved using Newton-Raphson technique in the following numerical form:

$$\sum_{l=2}^{n_y-1} \sum_{k=2}^{n_x-1} J_{k,l}^{i,j} \Delta \bar{P}_{k,l} = -F_{i,j}, \quad (5)$$

where, the Jacobian matrix is a tensorial quantity, given in terms of the residual derivatives as:

$$J_{k,l}^{i,j} = \frac{\partial F_{i,j}}{\partial P_{k,l}},$$

$F_{i,j}$ is a residual term and is explained in detail in [23–25].

Using the Gauss-Seidel iteration method, one can write Eq. (5) as:

$$\Delta P_{k,l}^n = \frac{-F_{i,j} - J_{k-1,l}^{i,j} \Delta P_{k-1,l}^n - J_{k+1,l}^{i,j} \Delta P_{k+1,l}^{n-1} - J_{k,l-1}^{i,j} \Delta P_{k,l-1}^n - J_{k,l+1}^{i,j} \Delta P_{k,l+1}^{n+1}}{J_{k,l}^{i,j}}. \quad (6)$$

The pressure can be updated using under-relaxation factor according to:

$$P_{i,j}^n = P_{i,j}^{n-1} + \Omega \Delta P_{i,j}^n, \quad (7)$$

where Ω is under-relaxation factor and its value equal 0.01.

The criterion for the pressure convergence is:

$$\left[\frac{\sum_i \sum_j (P_{i,j}^n - P_{i,j}^{n-1})^2}{M N} \right]^{0.5} \leq 10^{-3}. \quad (8)$$

The criterion for the load balance convergence is given as:

$$\left| \iint P(X, Y) dX dY - \frac{2}{3}\pi \right| \leq 10^{-4}, \quad (9)$$

where, M and N are the total nodal points in both the X and Y directions.

3. Results and discussion

To validate the current numerical solution for surface features conditions of a single ridge located at different position through the contact zone, a comparison have been made with the numerical results published by Venner and Lubrecht [10] and Holmes et al. [11] for the case where a transverse single ridge is located at different position through the contact zone. They modulated the single ridge as a cosine wave given with the formula:

$$S = A \cdot 10^{-10} \left[\frac{X - x_d}{\lambda} \right] \left(\cos 2\pi \frac{X - x_d}{\lambda} \right), \quad (10)$$

where A is the amplitude, λ is the wavelength of the ridge and x_d is the position where the ridge is located through the contact zone. The parameters chosen by Venner and Lubrecht [10] and Holmes et al. [11] are $A = 0.2 \mu\text{m}$ and $\lambda = 129 \mu\text{m}$. The pattern of the aforementioned ridge is shown in Fig. 1.

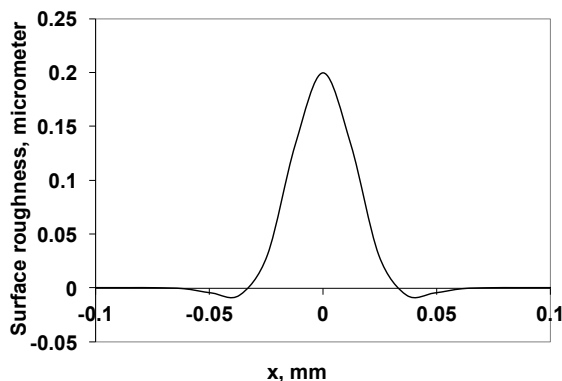


Fig. 1. Pattern of the ridge used by Venner and Lubrecht [10] and Holmes et al. [11]

The materials, lubricant and operating conditions are summarized in Table 1 for the numerical work reported by Venner and Lubrecht [10].

Table 1.

Geometry, material, lubricant properties and operating conditions

Viscosity η_0	1.22 Pa s	Radius of ball R_x	0.0127 m
Pressure of viscosity coefficient α	$2.2 \times 10^{-8} \text{ Pa}^{-1}$	Reduced modulus of elasticity E	$117 \times 10^9 \text{ Pa}$
ε	$5.83 \times 10^{-10} \text{ Pa}$	Load w	38 N
ξ	$1.68 \times 10^{-9} \text{ Pa}$	Speed u	0.01075 m/s

The data presented in Fig. 2 show the current numerical prediction of film thickness profile and pressure distribution in the direction of entraining motion through the central film when the ridge is located at different positions of $x_d = 0$, $-0.5b$ and $+0.5b$ through the contact zone for the pure rolling condition corresponding to the ridge located at the center of the contact, at the inlet of the contact and at the outlet of the contact, respectively, while those presented in Fig. 3 are the results obtained by numerical solution by Venner and Lubrecht [10] and Holmes et al. [11]. It is clear that the current numerical results presented in Fig. 2 conform well to those presented by numerical work of Venner and Lubrecht [10] and Holmes et al. [11]. It can be observed that the ridge completely flattens in the center of the contact (see Figs 2a and 3a) and only near the edge of the contact it affects the film thickness profile (see Figs 2b, 2c and 3b, 3c). In fact, the film thickness in the central region in Fig. 2a is uniform and its value, which is obtained from the current numerical results, is about $0.152 \mu\text{m}$, while that obtained from Venner and Lubrecht [10] results is about $0.15 \mu\text{m}$ (the error being about 1%). This flattening in film thickness in this region is followed by an increase in the pressure over the ridge in the center of the contact. According to Figs 2b and 3b, where the ridge is located at the inlet of the contact at a distance of $x_d = -0.5b$, the value of the film thickness in this region in the center of contact, obtained from the current numerical results, is about $0.147 \mu\text{m}$. As can be noticed, the film thickness in this region in the center of the contact decreases in comparison to that shown in Figs 2a and 3a. The physical explanation for this reduction in film thickness is attributed to the restriction on the lubricant flow into the contact due to the ridge existing at the inlet. The same behavior was observed also by Holmes et al. [11].

Fig. 4 shows the film thickness and pressure profile in the central line of the contact along the rolling direction obtained numerically for different amplitude values of the cosine-wave ridge ranging from $0.1 \mu\text{m}$ to $0.5 \mu\text{m}$ for the ridge located at different positions through the contact zone of $x_d = 0$, $-0.5b$ and $+0.5b$ under the same operating condition as mentioned before. It is clear that, as the amplitude of the ridge increases from $0.1 \mu\text{m}$ to $0.5 \mu\text{m}$, the maximum pressure over the ridge

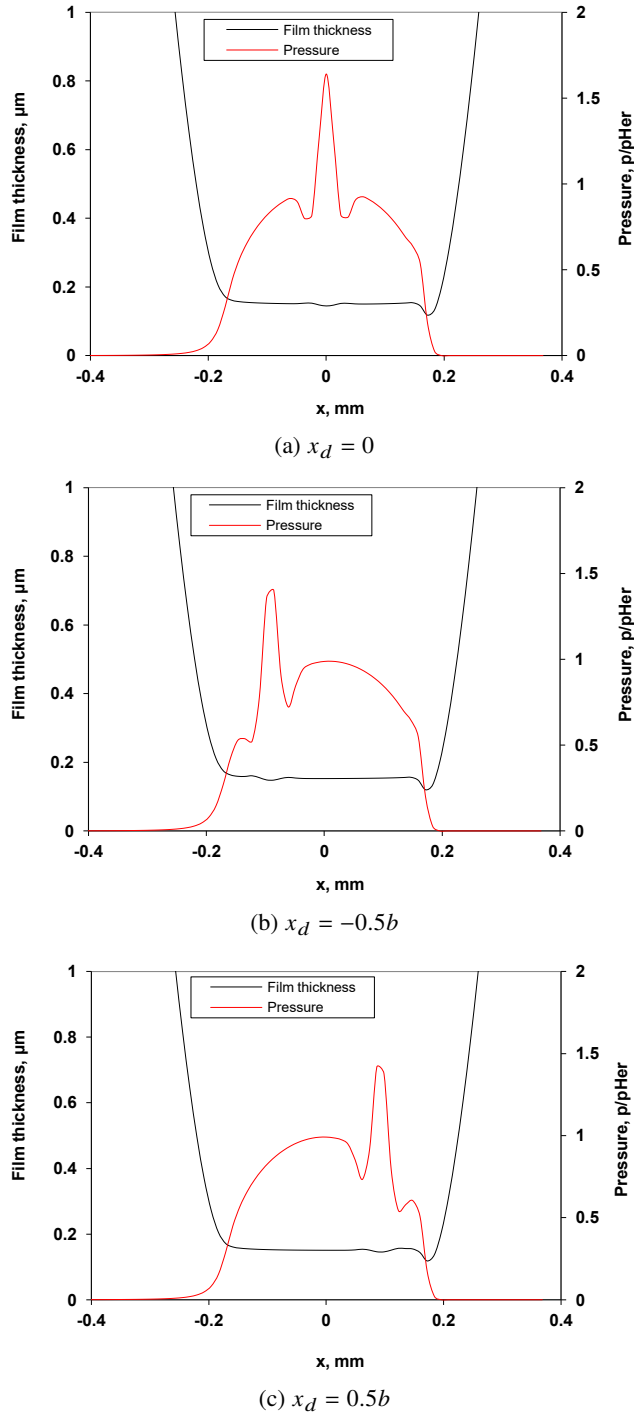
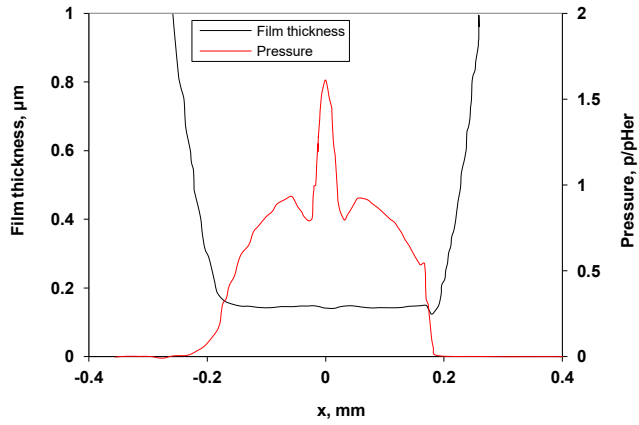
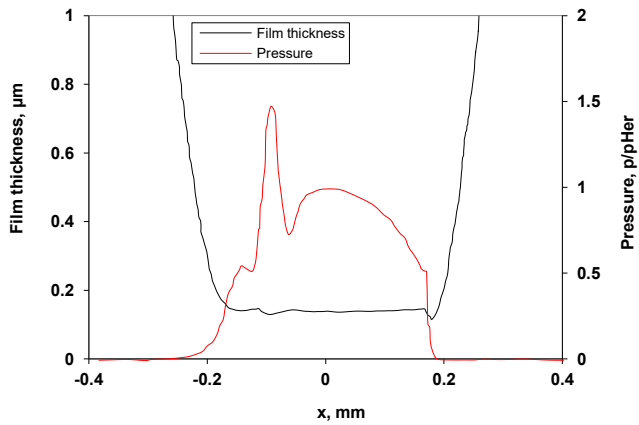


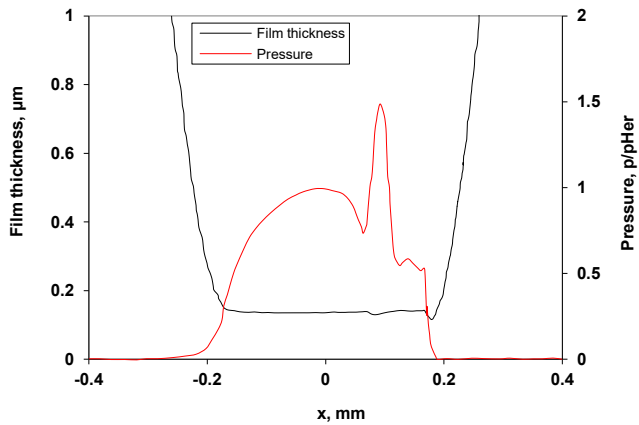
Fig. 2. Film profile and pressure for current numerical results at different ridge position



(a) $x_d = 0$

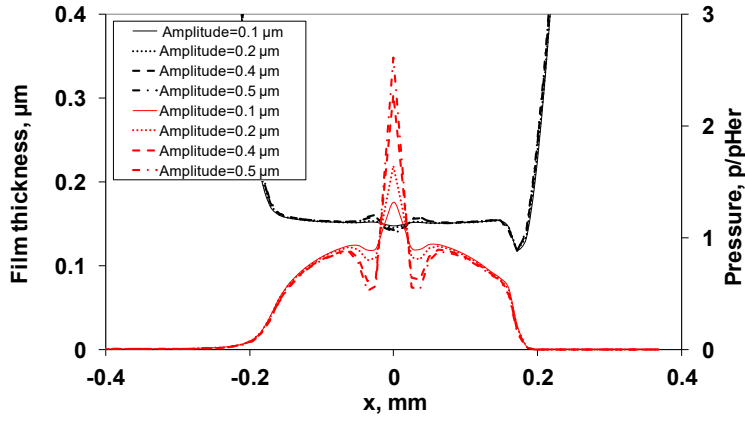


(b) $x_d = -0.5b$

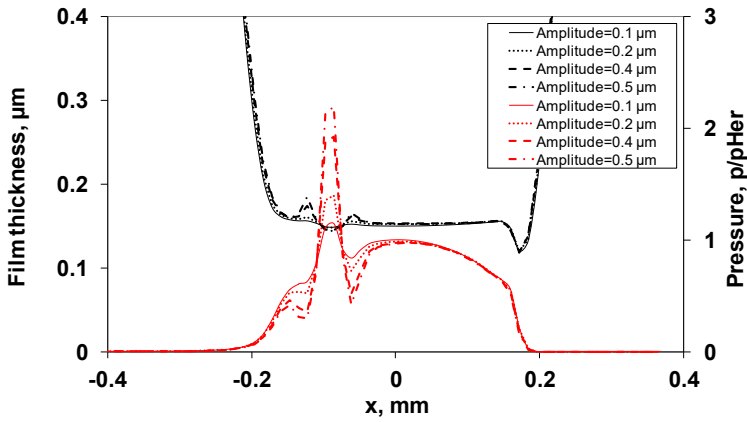


(c) $x_d = 0.5b$

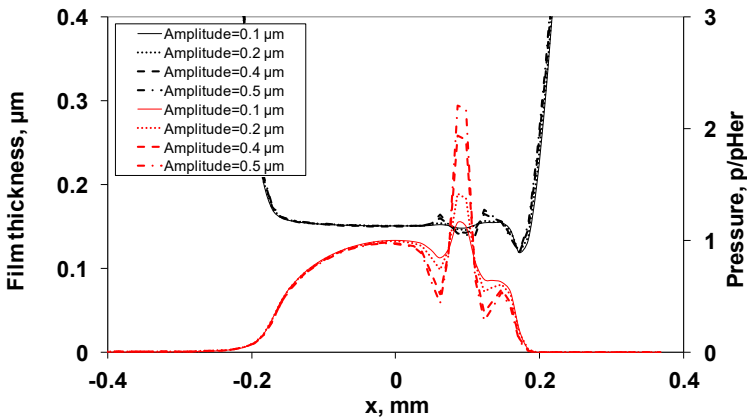
Fig. 3. Film profile and pressure after Holmes et al. [11] at different ridge position



(a) $x_d = 0$



(b) $x_d = -0.5b$



(c) $x_d = 0.5b$

Fig. 4. Film profile (black lines) and pressure (red lines) for different amplitudes of cosine wave ridge

increases (see Figs 4a, 4b and 4c. The film thickness profile through the contact zone, which forms corresponding to the ridge location at the inlet of the contact (i.e., at $x_d = -0.5b$), slightly decreases (see Fig. 4b). When the ridge is located at the center of the contact zone (i.e., at $x_d = 0$), the film thickness profile in the central region is uniform (see Fig. 4a). This feature is attributed to the completely deformed shape of the ridge profile.

The next step in this research is to study the behavior of steady-state elastohydrodynamic lubrication problems with artificial surface feature for different geometrical characteristics of the ridge patterns. In this case, a pattern of flat-top ridge and a sharp ridge pattern of triangular shape located at different position through the contact zone is considered through the following analysis to show the effects of variation of geometric characteristics of the ridge as well as the amplitude of the ridge on pressure and film profile. Fig. 5 shows the different ridge patterns used in the current analysis. Fig. 5a represents the flat-top pattern and Fig. 5b represents the sharp triangular ridge pattern.

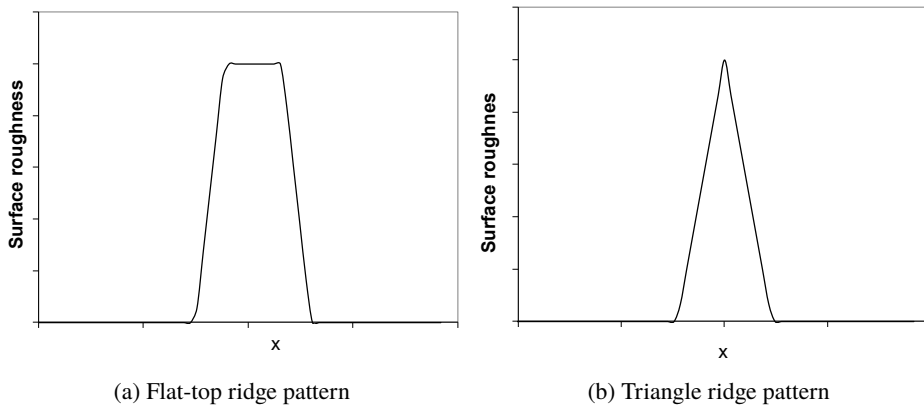
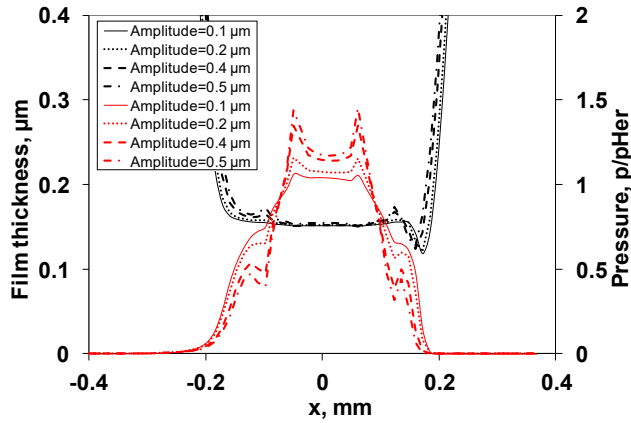
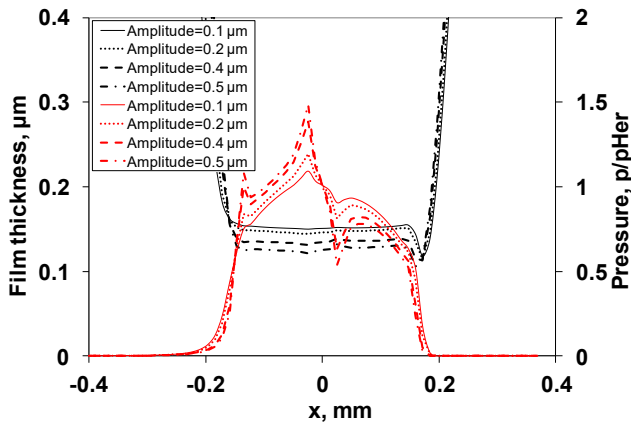


Fig. 5. Ridge pattern

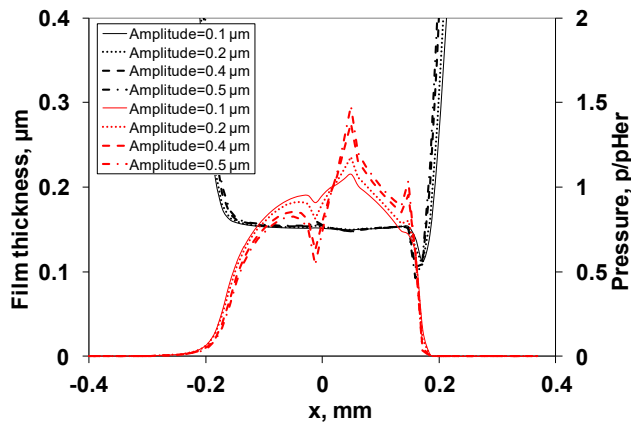
The data presented in Fig. 6 show the numerical prediction of the film thickness and pressure profile in the central line of contact along the rolling direction for a flat-top ridge shape located at different positions through an elastohydrodynamically lubricated contact of $x_d = 0, -0.5b, +0.5b$, corresponding to the location at the center of the contact, at the inlet of the contact and at the outlet of the contact, respectively, for operating conditions the same as used previously. The amplitude of the ridge used in the analysis varied from $0.1 \mu\text{m}$ to $0.5 \mu\text{m}$. It is clear that the variation of ridge amplitude from $0.1 \mu\text{m}$ to $0.5 \mu\text{m}$ causes that the amplitude of the pressure fluctuation over the ridge is more pronounced for a different ridge position. The locations of the ridge at the center of the contact and at the outlet of the contact have no effect on the central film thickness. In this case, the value of the film thickness in this region is about $0.15 \mu\text{m}$ for all values of amplitude variations, see Figs 6a and 6c. When the ridge is located at



(a) $x_d = 0$



(b) $x_d = -0.5b$



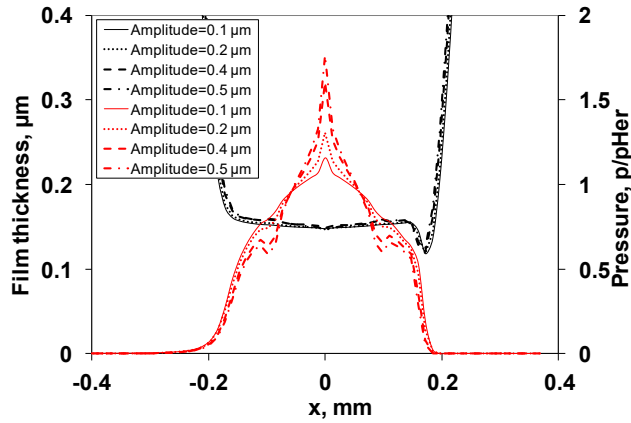
(c) $x_d = 0.5b$

Fig. 6. Film profile (black lines) and pressure (red lines) for flat-top ridge at different position

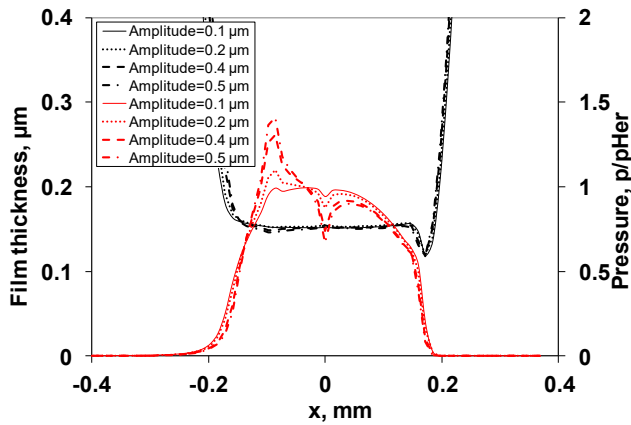
the inlet of the contact, the film thickness value is about $0.15 \mu\text{m}$ for ridge amplitude of $0.1 \mu\text{m}$ and this value decreases to about $0.12 \mu\text{m}$ as the ridge amplitude increases to about $0.5 \mu\text{m}$, see Fig. 6b. The explanation of the reduction of the film thickness when the ridge is located at the inlet of the contact is attributed to the restricted flow of the lubricant into the contact and this reduction in the amount of the lubricant flow increases as the amplitude increases. The result is the reduction in the film thickness in the central region. This analysis was supported by the results of other researchers, e.g., Venner and Lubrecht [10] and Holmes et al. [11].

Fig. 7 shows the numerical prediction of the film thickness and pressure profile in the central line of contact along the rolling direction for a sharp ridge of triangular shape located at different position through the elastohydrodynamically lubricated contact zone. The locations of the ridge are at $x_d = 0, -0.5b, 0.5b$, for operating conditions the same as previously used. The amplitude of the ridge used in the analysis varied from $0.1 \mu\text{m}$ to $0.5 \mu\text{m}$. It is clear that the amplitude of the pressure fluctuation over the ridge becomes greater as the amplitude of ridge increases for different positions of the ridge through the contact zone. The film thickness value in the center of the contact for a ridge positioned at the center of the contact and at the outlet of the contact is approximately $0.15 \mu\text{m}$, see Figs 7a and 7c for different amplitude values. When the ridge is located at the inlet of the contact, the film thickness is about $0.15 \mu\text{m}$ for a ridge amplitude of $0.1 \mu\text{m}$ and as the ridge amplitude increases to $0.5 \mu\text{m}$, the film thickness value in the center of the contact decreases to about $0.14 \mu\text{m}$.

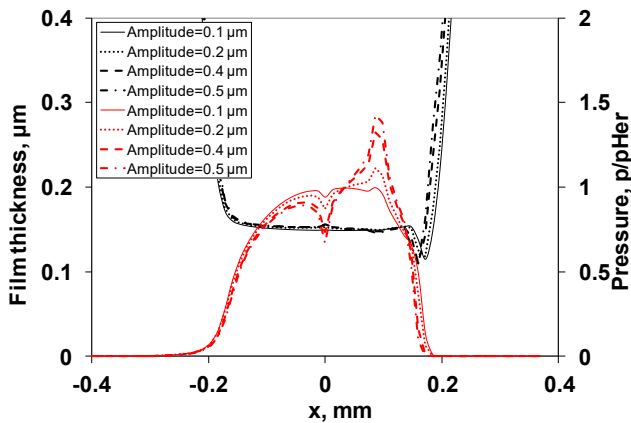
Finally, Fig. 8 shows a comparison of the film thickness with pressure profile in the central line of contact along the rolling direction obtained numerically for different ridge shapes, including cosine wave, flat-top and sharp triangular ridge pattern, located at different positions through the contact zone. Fig. 9 shows such a comparison for different types of ridge geometry used in the current analysis. The ridge amplitude is fixed at $0.5 \mu\text{m}$ to show the effect of changing ridge geometry on film thickness profile and pressure distribution. It is clear that the spike on pressure profile for the flat-top and the triangular shape is more pronounced in comparison to the cosine-wave ridge shape for different locations of the ridge (at the center of the contact or at the inlet of the contact or at the outlet of the contact). Finally, there appears the reduction in the film thickness as a result of formation of a dent in the film thickness. The film thickness profile presented in Fig. 8b shows that the film thickness in the center region for the flat-top ridge is reduced in comparison to that of the triangular ridge shape or the cosine ridge shape. The film thickness in this region is about $0.12 \mu\text{m}$ for the flat-top ridge, $0.14 \mu\text{m}$ for the triangular ridge shape and $0.15 \mu\text{m}$ for the cosine ridge shape. This effect can be attributed to the large amount of lubricant that is restricted to flow inside the contact zone because of the shape of the flat-top ridge.



(a) $x_d = 0$

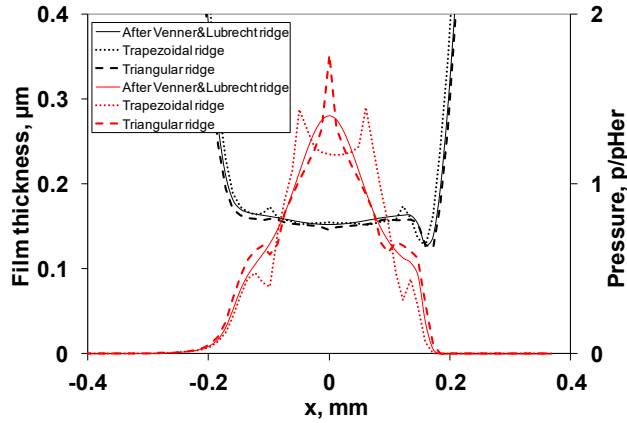


(b) $x_d = -0.5b$

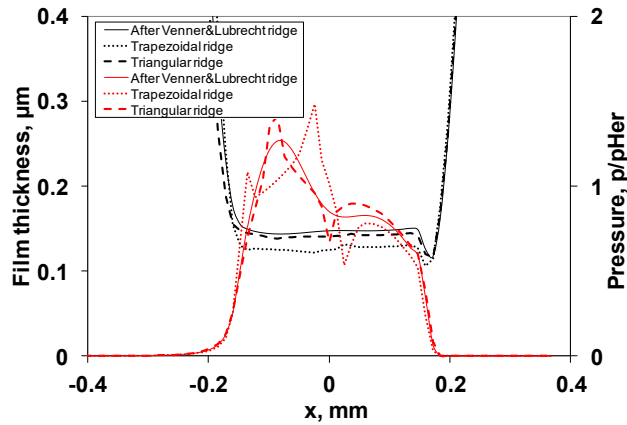


(c) $x_d = 0.5b$

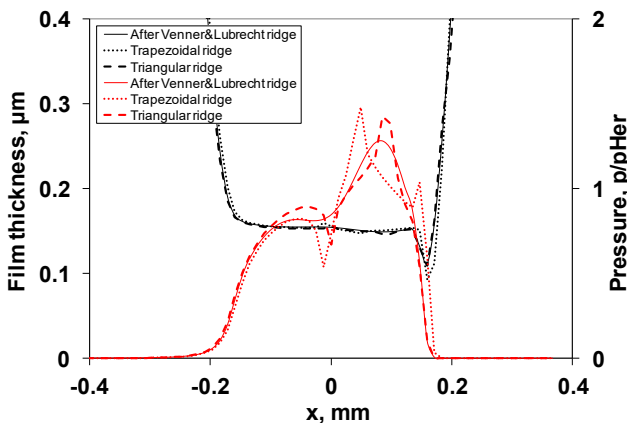
Fig. 7. Film profile (black lines) and pressure (red lines) for triangle ridge at different position



(a) $x_d = 0$



(b) $x_d = -0.5b$



(c) $x_d = 0.5b$

Fig. 8. Film profile (black lines) and pressure (red lines) for different ridge shape

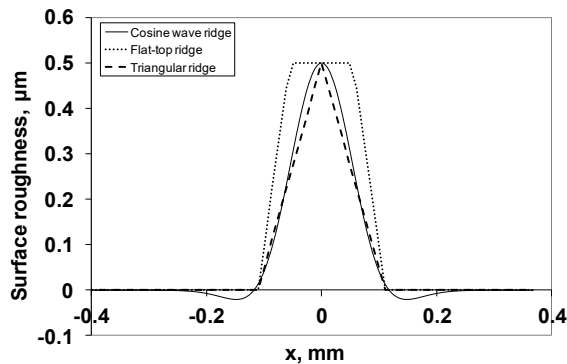


Fig. 9. Comparison of different ridge shape

4. Conclusions

The influence of geometric characteristics of the ridge, location of the ridge through the contact zone and the amplitude of the ridge on the elasto-hydrodynamic lubrication of point contact problem has been investigated in this paper. To study this behavior, a numerical solution using surfaces with artificial roughness with different ridge geometry and amplitude located at different position through elasto-hydrodynamic lubrication contacts has been developed to obtain the film thickness and the pressure distribution. The geometry of a single transverse ridge across the contact zone was simulated and the Newton-Raphson technique with Gauss-Seidel iteration method was used to solve the Reynolds equation. The results showed that one should select the geometrical characteristics of the ridge which have profiles with smooth transitions with an appropriate amplitude to reduce the pressure spike and, therefore, to minimize wear, friction and to increase fatigue life. The location of the ridge with respect to the contact zone, as well as the amplitude of the ridge, play an important role in the formation of lubricant film thickness profile and the pressure distribution through the contact zone. Finally, the obtained numerical results have been compared with other published numerical results and show a good agreement.

Manuscript received by Editorial Board, May 30, 2020;
final version, November 21, 2020.

References

- [1] R. Gohar and H. Rahnejat. *Fundamentals of Tribology*. Imperial College Press, London, 2008.
- [2] N. Patir and H.S. Cheng. An average flow model for determining effects of three-dimensional roughness on partial hydrodynamic lubrication. *Journal of Lubrication Technology*, 100(1):12–17, 1978. doi: [10.1115/1.3453103](https://doi.org/10.1115/1.3453103).

- [3] D. Epstein, T. Yu, Q.J. Wang, L.M. Keer, H.S. Cheng, S. Liu, S.J. Harris, and A. Gangopadhyay. An efficient method of analyzing the effect of roughness on fatigue life in mixed-EHL contact. *Tribology Transactions*, 46(2):273–281, 2003. doi: [10.1080/10402000308982626](https://doi.org/10.1080/10402000308982626).
- [4] Q.J. Wang, D. Zhu, H.S. Cheng, T. Yu, X. Jiang, and S. Liu. Mixed lubrication analyses by a macro-micro approach and a full-scale mixed EHL model. *Journal of Tribology*, 126(1):81–91, 2004. doi: [10.1115/1.1631017](https://doi.org/10.1115/1.1631017).
- [5] M. Masjedi and M.M. Khonsari. On the effect of surface roughness in point-contact EHL: formulas for film thickness and asperity load. *Tribology International*, 82(Part A):228–244, 2015. doi: [10.1016/j.triboint.2014.09.010](https://doi.org/10.1016/j.triboint.2014.09.010).
- [6] Y.Z. Hu and D. Zhu. A full numerical solution to the mixed lubrication in point contacts. *Journal of Tribology*, 122(1):1–9, 2000. doi: [10.1115/1.555322](https://doi.org/10.1115/1.555322).
- [7] B. Jacod, C.H. Venner, and P.M. Lugt. Influence of longitudinal roughness on friction in EHL contacts. *Journal of Tribology*, 126(3):473–481, 2004. doi: [10.1115/1.1705664](https://doi.org/10.1115/1.1705664).
- [8] P. Yang, J. Cui, Z.M. Jin, and D. Dowson. Influence of two-sided surface waviness on the EHL behavior of rolling/sliding point contacts under thermal and non-Newtonian conditions. *Journal of Tribology*, 130(4):041502, 2008. doi: [10.1115/1.2958078](https://doi.org/10.1115/1.2958078).
- [9] J. Wang, C.H. Venner, and A.A. Lubrecht. Amplitude reduction in EHL line contacts under rolling sliding conditions. *Tribology International*, 44(12):1997–2001, 2011. doi: [10.1016/j.triboint.2011.08.009](https://doi.org/10.1016/j.triboint.2011.08.009).
- [10] C.H. Venner and A.A. Lubrecht. Numerical simulation of a transverse ridge in a circular EHL contact under rolling/sliding. *Journal of Tribology*, 116(4):751–761, 1994. doi: [10.1115/1.2927329](https://doi.org/10.1115/1.2927329).
- [11] M.J.A. Holmes, H.P. Evans, T.G. Hughes, and R.W. Snidle. Transient elastohydrodynamic point contact analysis using a new coupled differential deflection method Part 1: Theory and validation. *Proceedings of the Institution of Mechanical Engineers, Part J: Journal of Engineering Tribology*, 217(4):289–304, 2003. doi: [10.1243/135065003768618641](https://doi.org/10.1243/135065003768618641).
- [12] A. Félix-Quíñonez, P. Ehret, and J.L. Summers. Numerical analysis of experimental observations of a single transverse ridge passing through an elastohydrodynamic lubrication point contact under rolling/sliding conditions. *Proceedings of the Institution of Mechanical Engineers, Part J: Journal of Engineering Tribology*, 218(2):109–123, 2004. doi: [10.1177/135065010421800206](https://doi.org/10.1177/135065010421800206).
- [13] A. Félix-Quíñonez, P. Ehret, J.L. Summers, and G.E. Morales-Espejel. Fourier analysis of a single transverse ridge passing through an elastohydrodynamically lubricated rolling contact: a comparison with experiment. *Proceedings of the Institution of Mechanical Engineers, Part J: Journal of Engineering Tribology*, 218(1):33–43, 2004. doi: [10.1243/135065004322842816](https://doi.org/10.1243/135065004322842816).
- [14] M. Kaneta, H. Nishikawa and K. Matsuda. Behaviour of transverse ridges passing through a circular EHL conjunction. In: Snidle R.W., Evans H.P. (eds) *IUTAM Symposium on Elastohydrodynamics and Micro-elastohydrodynamics*, pages 189–200, Cardiff, UK, 1–3 September, 2004. doi: [10.1007/1-4020-4533-6_13](https://doi.org/10.1007/1-4020-4533-6_13).
- [15] I. Křupka, M. Hartl, L. Urbanec, and J. Čermák. Single dent within elastohydrodynamic contact – comparison between experimental and numerical results. *Proceedings of the Institution of Mechanical Engineers, Part J: Journal of Engineering Tribology*, 221(6):635–644, 2007. doi: [10.1243/13506501JET276](https://doi.org/10.1243/13506501JET276).
- [16] X. Feng Wang, R.F. Hu, W. Shang and F. Zhao. Experimental and numerical investigation on single dent with marginal bump in EHL point contacts. *Industrial Lubrication and Tribology*, 69(2):798–807, 2017.
- [17] I. Ficza, P. Sperka, and M. Hartl. Transient calculations in elastohydrodynamically lubricated point contacts. *Engineering Mechanics*, 21(5):311–319, 2014.

- [18] P. Sperka. *In-situ studium zmeny topografie trecích povrchu v elastohydrodynamickém kontaktu (In-situ Study of Surface Topography changes in Elastohydrodynamic Contact)*. Ph.D. Thesis. Brno University of Technology, Czech Republic, 2011. (in Czech).
- [19] F. Ali, M. Kaneta, I. Křupka, and M. Hartl. Experimental and numerical investigation on the behavior of transverse limited micro-grooves in EHL point contacts. *Tribology International*, 84:81–89, 2015. doi: [10.1016/j.triboint.2014.11.025](https://doi.org/10.1016/j.triboint.2014.11.025).
- [20] P. Sperka, I. Křupka, and M. Hartl. Prediction of shallow indentation effects in a rolling-sliding ehl contact based on amplitude attenuation theory. *Tribology Online*, 12(1):1–7, 2017. doi: [10.2474/trol.12.1](https://doi.org/10.2474/trol.12.1).
- [21] D. Kostal, P. Sperka, I. Křupka, and M. Hartl. Artificial surface roughness deformation in the starved EHL contacts. *Tribology Online*, 13(1):1–7, 2018. doi: [10.2474/trol.13.1](https://doi.org/10.2474/trol.13.1).
- [22] T. Hultqvist, A. Vrcek, P. Marklund, B. Prakash, and R. Larsson. Transient analysis of surface roughness features in thermal elastohydrodynamic contacts. *Tribology International*, 141:105915, 2020. doi: [10.1016/j.triboint.2019.105915](https://doi.org/10.1016/j.triboint.2019.105915).
- [23] M.F. Al-Samieh and H. Rahnejat. Nano-lubricant film formation due to combined elastohydrodynamic and surface force action under isothermal conditions. *Proceedings of the Institution of Mechanical Engineers, Part C: Journal of Mechanical Engineering Science*, 215(9):1019–1029, 2001. doi: [10.1177/095440620121500902](https://doi.org/10.1177/095440620121500902).
- [24] M.F. Al-Samieh. Effect of changing ellipticity ratio on the formation of ultra-thin lubricating film. *Tribology in Industry*, 39(4):431–443, 2017. doi: [10.24874/ti.2017.39.04.02](https://doi.org/10.24874/ti.2017.39.04.02).
- [25] M.F. Al-Samieh. Surface roughness effects for newtonian and non-Newtonian lubricants. *Tribology in Industry*, 41(1):56–63, 2019. doi: [10.24874/ti.2019.41.01.07](https://doi.org/10.24874/ti.2019.41.01.07).
- [26] D. Dowson and G.R. Higginson. A numerical solution to the elastohydrodynamic problem. *Journal of Mechanical Engineering Science*, 1(1):6–15, 1959. doi: [10.1243/JMES_JOUR_1959_001_004_02](https://doi.org/10.1243/JMES_JOUR_1959_001_004_02).
- [27] C.J.A. Roelands. *Correlation aspects of viscosity-temperature-pressure relationship of lubricating oils*. Ph.D. Thesis. Delft University of Technology, The Netherlands, 1966.